3-9-2010

Atomic details of near-transition state conformers for enzyme phosphoryl transfer revealed by MgF_3^- rather than by phosphoranes

Nicola J. Baxter
University of Sheffield

Matthew W. Bowler
European Synchrotron Radiation Facility

Tooba Alizadeh
University of Sheffield

Matthew J. Cliff
University of Sheffield

Andrea M. Hounslow
University of Sheffield

See next page for additional authors

Authors
Nicola J. Baxter, Matthew W. Bowler, Tooba Alizadeh, Matthew J. Cliff, Andrea M. Hounslow, Bin Wu, David B. Berkowitz, Nicholas H. Williams, G. Michael Blackburn, and Jonathan P. Waltho

Atomic details of near-transition state conformers for enzyme phosphoryl transfer revealed by MgF_3^- rather than by phosphoranes

Nicola J. Baxter[a], Matthew W. Bowler[b], Tooba Alizadeh[a], Matthew J. Cliff[a], Andrea M. Hounslow[a], Bin Wu[c], David B. Berkowitz[c], Nicholas H. Williams[d], G. Michael Blackburn[a,2], and Jonathan P. Waltho[a,e,2]

[a]Department of Molecular Biology and Biotechnology, University of Sheffield, Sheffield S10 2TN, United Kingdom; [b]Structural Biology Group, European Synchrotron Radiation Facility, 6 rue Jules Horowitz, F-38043 Grenoble, France; [c]Department of Chemistry, University of Nebraska-Lincoln, Lincoln, NE 68588; [d]Centre for Chemical Biology, Department of Chemistry, University of Sheffield, Sheffield S3 7HF, United Kingdom; and [e]Faculty of Life Sciences and Manchester Interdisciplinary Biocentre, University of Manchester, Manchester, M1 7DN, United Kingdom

Communicated by Paul Zamecnik, Massachusetts General Hospital, Charlestown, MA, September 16, 2009 (received for review June 2, 2009)

Prior evidence supporting the direct observation of phosphorane intermediates in enzymatic phosphoryl transfer reactions was based on the interpretation of electron density corresponding to trigonal species bridging the donor and acceptor atoms. Close examination of the crystalline state of β-phosphoglucomutase, the archetypal phosphorane intermediate-containing enzyme, reveals that the trigonal species is not PO_3^-, but is MgF_3^- (trifluoromagnesate). Although MgF_3^- complexes are transition state analogues rather than phosphoryl group transfer reaction intermediates, the presence of fluorine nuclei in near-transition state conformations offers new opportunities to explore the nature of the interactions, in particular the independent measures of local electrostatic and hydrogen-bonding distributions using ^{19}F NMR. Measurements on three β-PGM-MgF_3^--sugar phosphate complexes show a remarkable relationship between NMR chemical shifts, primary isotope shifts, NOEs, cross hydrogen bond F···H-N scalar couplings, and the atomic positions determined from the high-resolution crystal structure of the β-PGM-MgF_3^--G6P complex. The measurements provide independent validation of the structural and isoelectronic MgF_3^- model of near-transition state conformations.

19F NMR | phosphoryl transfer enzyme | transition state analogue | trifluoromagnesate

The mono- and diesters of phosphoric acid have commanding and ubiquitous roles in all species of life. As structural components they show remarkable stability to spontaneous hydrolysis under near physiological conditions (25 °C), with half-lives for P-O bond cleavage in phosphate diesters estimated at *ca.* 10^7 years and for monoesters *ca.* 10^{12} years (1, 2). Yet, they are susceptible to enzyme-catalyzed hydrolysis and phosphoryl group transfer reactions either between two oxygens, or between oxygen and nitrogen or sulfur, with turnover numbers adequate to support a vast array of biological processes, e.g. *Serratia* nuclease k_{cat} *ca.* $2,500\ s^{-1}$ (3), *E. coli* alkaline phosphatase $k_{cat} \geq 45\ s^{-1}$ (4), and human protein tyrosine phosphatase β k_{cat} *ca.* $1,500\ s^{-1}$ (5). Such values lead to the remarkable result that phosphoryl transfers involved in cell signaling and regulation are associated with the largest enzymatic rate enhancements yet identified (2), with accelerations k_{cat}/k_{uncat} in the range 10^{21}. Two general properties of phosphate esters are largely responsible for their stability: anionic character and aqueous solvation (6). Both of these deter nucleophilic attack at phosphorus and have to be overcome by enzyme catalysts. While the generalities of enzyme catalysis of phosphoryl group transfer have been well established by stereochemical studies and analysis of nucleophile and leaving group dependencies, in conjunction with much structural information (6), detailed knowledge of transition states (TSs) for reactions of true substrates has been difficult to establish. In this regard, trifluoromagnesate (MgF_3^-) has recently emerged as a surrogate for the PO_3^- group in enzyme TSs (7–9), and is the likely species present in many reported near-TS structures previously thought to contain AlF_3 (10). Here we show, using a combination of solution NMR and high-resolution x-ray crystallography applied to the enzyme β-phosphoglucomutase (β-PGM), that MgF_3^- provides a very sensitive probe of the electrostatic and hydrogen-bonding distributions in a near-TS conformation. MgF_3^- is isoelectronic with, and a close steric mimic of, an enzyme-bound PO_3^- moiety.

Two very different PGM families exist; one operates on α-D-glucose 1-phosphate and one on β-D-glucose 1-phosphate (βG1P). α-Phosphoglucomutase, (α-PGM, EC 5.4.2.2), a key enzyme in glycolysis (11), has long been established as requiring α-D-glucose 1,6-bisphosphate (αG16BP) as a cofactor to convert the apoenzyme into the catalytically active form. This involves the phosphorylation of a conserved serine (S116 in α-PGM from rabbit muscle) to give a stable phosphate monoester ($k_{hydrolysis} = 3.3 \times 10^{-8}\ s^{-1}$ for phosphate hydrolysis (12)) and glucose 6-phosphate (G6P) as product. The bacterial β-phosphoglucomutases (β-PGM, EC 5.4.2.6) are smaller proteins, operate on βG1P, and use a conserved aspartate (D8 in β-PGM from *L. lactis*) as a nucleophile to form a transient phospho-enzyme (13). The short lifetime of the phospho-enzyme ($k_{hydrolysis} = 0.05\ s^{-1}$ (14); $0.026 \pm 0.001\ s^{-1}$ (15)) is unsurprising because acyl phosphates are highly reactive phosphorylating species ($\Delta G^{\circ}_{hydrolysis} = -10$ kcal mol^{-1}). Only in exceptional circumstances are the half-lives extended above 24 h (16).

Investigation of the mechanism of β-PGM was set alight by the claimed observation of a pentacovalent phosphorane intermediate formed from β-PGM and βG1P or G6P (17). Because of inconsistencies in the interpretation of the high-resolution x-ray data and in the thermodynamic justification of the proposed phosphorane, we immediately suggested an alternative interpretation of the electron density map as resulting from an MgF_3^- anion occupying the active site with G6P (18). The MgF_3^- interpretation received independent support from a quantum

Author contributions: N.J.B., M.W.B., M.J.C., A.M.H., N.H.W., G.M.B., and J.P.W. designed research; N.J.B., M.W.B., T.A., M.J.C., A.M.H., and J.P.W. performed research; B.W. and D.B.B. contributed new reagents/analytic tools; N.J.B., M.W.B., M.J.C., G.M.B., and J.P.W. analyzed data; and N.J.B., M.W.B., G.M.B., and J.P.W. wrote the paper.

The authors declare no conflict of interest.

Data deposition: The atomic coordinates and structure factors for the PGM-MgF_3-G6P-TSA complex and native β-PGM in the open unphosphorylated state have been deposited in the Protein Data Bank, www.pdb.org (PDB ID codes 2wf5 and 2whe). The NMR chemical shifts have been deposited in the BioMagResBank, www.bmrb.wisc.edu (accession nos. 7234 and 7235).

[1]N.J.B. and M.W.B. contributed equally to this work.

[2]To whom correspondence should be addressed. E-mail: j.waltho@sheffield.ac.uk or g.m.blackburn@sheffield.ac.uk.

This article contains supporting information online at www.pnas.org/cgi/content/full/0910333106/DCSupplemental.

BIOCHEMISTRY

mechanical - molecular mechanical (QM-MM) analysis based on the structure (19) and was subsequently validated in solution by direct observation based on ^{19}F NMR data (8). However, the MgF_3^- interpretation was questioned (20, 21) and the pentacovalent phosphorane interpretation defended (22, 23), despite the presence of fluoride, which severely compromises the catalytic cycle of β-PGM (15). Therefore, using an integration of NMR and high-resolution x-ray structural data, we now report a thorough characterization of β-PGM in the presence of G6P and fluoride that leaves no room for a pentacovalent phosphorane interpretation of solid-state or solution-state complexes. It also demonstrates the substantial role to be played by ^{19}F NMR parameters in the characterization of metal fluoride transition state analogue (TSA) complexes.

Results and Discussion

The presence of the reported pentacovalent phosphorane species (17) relies on the accumulation of β-PGM phosphorylated on D8 with which either G6P or βG1P can associate to form the proposed high-energy reaction intermediate. We investigated the potential for β-PGM to accumulate a population of phosphoenzyme using ^{31}P NMR (see *SI Text*). The ^{31}P NMR spectrum of β-PGM expressed and purified according to established procedures (13, 24) showed that freshly prepared protein has no phosphate moiety. The addition of either G6P or βG1P to a solution of unliganded β-PGM, replicating the original crystallization conditions (17) (except that fluoride was omitted), failed to show any phosphorus species covalently bound to protein, as predicted by the detailed kinetic analysis of β-PGM (15). Under these conditions, there was also no measureable population of noncovalently bound sugar phosphate (only free G6P as α- and β-anomers, free Pi derived from the slow hydrolysis of G6P (15), and several other minor non-protein-bound sugar phosphates were observed). The subsequent inclusion of 10 mM ammonium fluoride (Fig. 1) resulted in the formation of the previously described PGM-MgF_3-G6P-TSA complex (8), and the observation of a protein-bound phosphate resonance from G6P in the complex (with an intensity proportional to the protein concentration). No peaks were observed at chemical shifts characteristic of a protein-bound aspartyl phosphate (25) or of a pentacoordinate phosphorane species (26), both of which would occur at higher field than Pi. Furthermore, the remarkable hypothesis that the presence of Pi is sufficient to cause phosphorylation of D8 before or after crystallization (14), can also be discounted by ^{31}P NMR showing the absence of an aspartyl phosphate peak in the presence of a large excess of Pi (Fig. 1). The observation that native β-PGM is not phosphorylated is also supported by electrospray mass-spectrometric analysis (8).

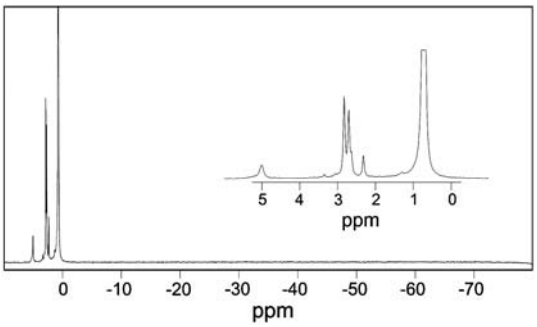

Fig. 1. A ^{31}P NMR spectrum of the crystallization components, including β-PGM, G6P, $MgCl_2$ and NH_4F. The spectrum shows (expanded in inset) resonances of the protein-bound phosphate from G6P in the PGM-MgF_3-G6P-TSA complex (5.00 ppm), free G6P in solution as α- and β-anomers (2.70 and 2.82 ppm, respectively) and free Pi (0.72 ppm), as well as minor amounts of several other non-protein-bound sugar phosphates. No other peaks are observed at chemical shifts resonating upfield of Pi characteristic of a protein-bound aspartyl phosphate or a pentacoordinate phosphorane species.

X-ray analysis of crystals of freshly purified β-PGM further established that the protein is not phosphorylated on D8. We crystallized β-PGM in the absence of ligands and determined the structure to a resolution of 1.55 Å (Table S1). The protein is in an open conformation that is essentially the same as that reported previously (14), with root mean square (RMS) deviations of 0.78 Å for all main-chain atoms. Analysis of the difference Fourier maps showed no density near to the catalytic aspartyl carboxylate moiety (Fig. S1). This observation contrasts with the original report (13) of the isolation and crystallization of β-PGM phosphorylated on D8. However, at the resolution then reported (2.3 Å), other interpretations of electron density in the vicinity of D8 are equally valid. It is particularly likely that the observed density is the result of the formation of an aluminum fluoride adduct of β-PGM. The population of such an adduct, in the absence of other ligands, was established using ^{19}F NMR (Fig. S2). Although the crystallization conditions reported contained no added aluminum, the levels of fluoride used (100 mM) are sufficient to leach aluminum from laboratory glassware, as shown previously (27, 28).

In the presence of G6P, magnesium and fluoride, β-PGM readily forms a PGM-MgF_3-G6P-TSA complex in solution. However, the possibility that the solution-state and solid-state species differ still needs to be considered. Hence, we crystallized β-PGM in the presence of G6P and fluoride under conditions as close as possible to those used in the solution NMR study and we solved the structure to a resolution of 1.3 Å (Table S1). The protein is in a closed conformation that is essentially the same as that reported to contain the pentacovalent phosphorane intermediate (17), with RMS deviations of 0.4 Å for all main-chain atoms. The difference Fourier map showed clear density for G6P and a trigonal planar species (Fig. S3). The building of a model with MgF_3^- as the trigonal species, provided a very good fit to the density with bond lengths very similar to those of typical Mg-F bonds (1.90 to 2.03 Å (29)). The resolution to which our data were collected (1.3 Å) allowed us to refine the positions of the atoms without any bond length and angle restraints. This assigns the trigonal bipyramid (TBP) equatorial bond lengths as (Mg-F_A = 1.8 Å, Mg-F_B = 1.8 Å, Mg-F_C = 1.9 Å), which is inconsistent with previously reported P-O bond lengths. Furthermore, to investigate independently the identity of the central atom of the trigonal planar species, a dataset was collected at a wavelength of 1.77 Å (E = 7 keV) on a crystal from the same drop as the native dataset (Table S1). At this wavelength the anomalous scattering lengths from light elements (such as phosphorus and sulfur) are much longer than at shorter wavelengths (Note: the scattering factors ($\Delta f''$) for P at 1.77 Å ($\Delta f''$ = 0.56 electrons) will be a factor of 4 greater than at 0.9 Å ($\Delta f''$ = 0.15 electrons), where previously reported anomalous scattering measurements were attempted (17, 20). The scattering factor for magnesium is too small to observe a signal at either wavelength ($\Delta f''$ = 0.23 electrons at 1.77 Å and 0.06 electrons at 0.9 Å). Inspection of the anomalous difference Fourier map calculated from these data with phases from a refined model at a contour level of 3σ (Table S2) showed four clear peaks: three peaks at the methionine side-chain sulfur atoms of M1, M83, and M126 and one peak on the phosphorus atom of G6P in the complex (Fig. 2*A*). No other peaks were present. (See Table S2 for details of the observed peak heights in the anomalous difference Fourier maps compared to the anomalous scattering factors for these elements.) Therefore, by combining the crystal structure and the ^{19}F NMR data (8) with the anomalous scattering data, the TBP species observed in this crystal structure is unambiguously defined as pentacoordinate trifluoromagnesate (MgF_3^-).

The apparent differences between the interpretation of data described above and that previously reported for the proposed

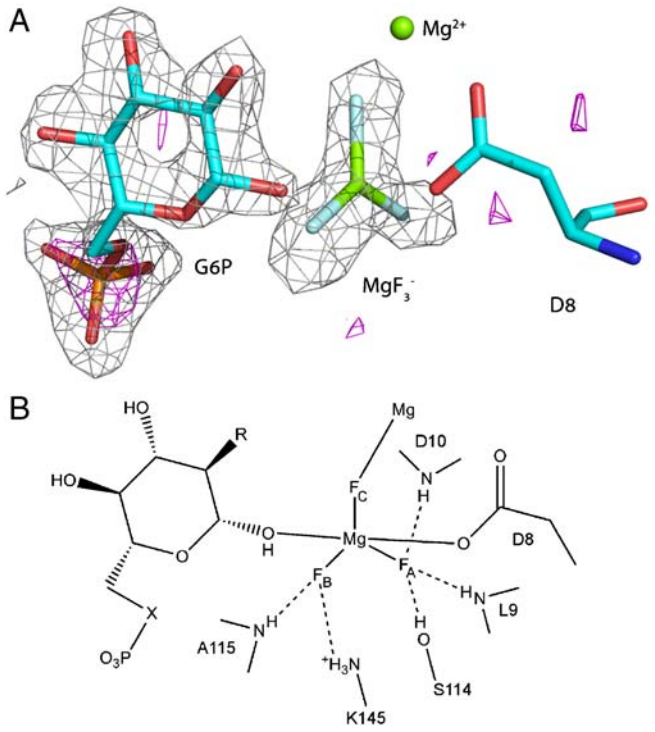

Fig. 2. Structure of the PGM-MgF_3-G6P-TSA complex active site. (*A*) The difference Fourier map and the anomalous substructure of the PGM-MgF_3-G6P-TSA complex. Anomalous difference density contoured at 3σ is shown as a *magenta mesh*. A large peak (height 7.1σ) is visible for the phosphorus atom in G6P. No corresponding phosphorus peak was observed in the active site confirming the assignment of the trigonal planar species as MgF_3^- and not PO_3^-. The difference electron density ($F_o - F_c$) from the same data is shown as a *gray mesh* contoured at 3σ for G6P and the MgF_3^- moiety before their inclusion in the model. (*B*) Schematic view of the PGM-MgF_3-sugar phosphate-TSA complex active site. Three sugar moieties were studied: G6P (R = OH, X = O); 6-deoxy-6-(phosphonomethyl)-D-glucopyranoside (R = OH, X = CH_2); 2-deoxy-G6P (R = H, X = O).

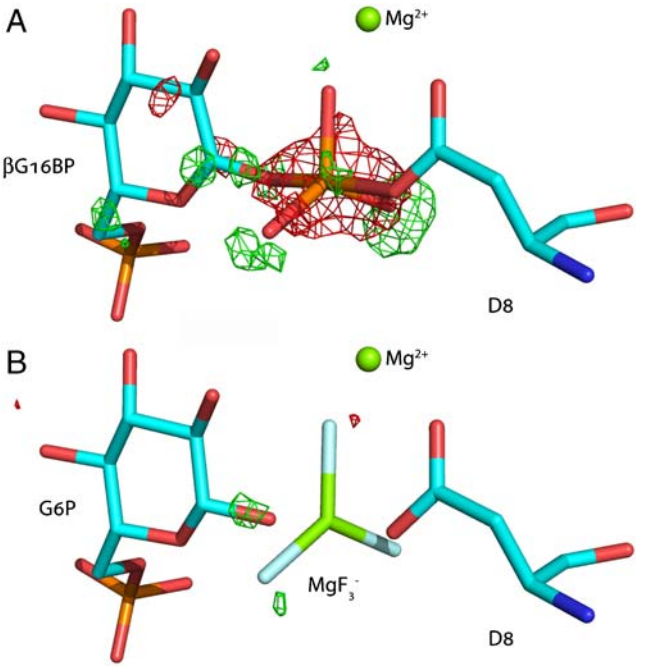

Fig. 3. The reported pentacovalent phosphorus intermediate with β-PGM (17) is a PGM-MgF_3-G6P-TSA complex. (*A*) Difference Fourier maps calculated for the structure 1o08 contoured at $+3\sigma$ and -3σ. The difference maps show significant discrepancies from the original interpretation (17) in the derived bond lengths and assignment of atoms in the TBP moiety. Positive peaks (*ca*. 8σ, *green*) are observed beyond each of the equatorial atoms of the TBP indicating that the assigned equatorial bond lengths were too short. The large negative peak (9.6σ, *red*) for the central coordinating atom indicates that the true atomic species is lighter than phosphorus. (*B*) Difference Fourier maps calculated after refinement against the deposited structure factors (www.pdb.org) with MgF_3^- replacing PO_3^- as the trigonal planar species. Unrestrained refinement of the deposited coordinates against the deposited structure factors leads to equatorial bond lengths of *ca.* 1.9 Å, which are consistent with our observed bond lengths. Replacing PO_3^- with MgF_3^- as the trigonal planar species in the model eliminates peaks in the difference Fourier maps above 3σ.

pentacovalent phosphorane are readily resolved. Inspection of the difference Fourier maps calculated after refinement of structure 1o08 against the deposited structure factors (www.pdb.org) shows significant discrepancies from the original interpretation in the derived bond lengths and assignment of atoms in the TBP moiety (17). In the difference map (Fig. 3*A*, Fig. S4), positive peaks (*ca*. 8σ) are observed beyond each of the equatorial atoms of the TBP indicating that the assigned atoms were incorrectly located (i.e. the assigned equatorial bond lengths were too short). Furthermore, a large negative peak (9.6σ) is observed for the central coordinating atom indicating that the true atomic species is lighter than phosphorus. Unrestrained refinement of the deposited coordinates against the deposited structure factors leads to equatorial bond lengths of 1.9 Å, which are consistent with our observed bond lengths. Refinement replacing PO_3^- by MgF_3^- as the trigonal planar species eliminates peaks in the difference Fourier maps greater than 3σ (Fig. 3*B*, Fig. S5). (Note: while it is possible to discern the difference between Mg and P experimentally, F and O are indistinguishable.) Hence, given a population of MgF_3^- stoichiometric with the protein concentration (8) in the original crystallization conditions (17), the accurate interpretation of the electron density is a PGM-MgF_3-G6P-TSA complex.

Although MgF_3^- complexes are TSAs rather than phosphoryl group transfer reaction intermediates, the presence of fluorine nuclei in near-TS conformations offers unique opportunities to explore the nature of the interactions. Because the lifetimes for enzymatic phosphoryl transfer TSs are so short, structural analysis of the protein-TS interface is currently most effectively carried out in complexes of enzymes with TSAs, where the TSAs have very high affinity for the active site and close mimicry of the electronic and geometric character of the TS (30). Notably, MgF_3^- is isoelectronic with the metaphosphate anion (PO_3^-), both species having 24 electrons in the valence shell, one net negative charge, and being capable of accepting two apical ligands to generate pentacoordinate TBP geometry. Such a close relationship between the TS and TSA for phosphoryl transfer is virtually unattainable for other enzyme-catalyzed reactions. While this mimicry can be accurately mapped in high-resolution x-ray protein structures for the solid state (7, 9), the ^{19}F atoms are ideal for the NMR investigation of multiple features of the near-TS species in the solution phase.

The first key probe of the interactions within the TSA is provided by the ^{19}F chemical shifts, which report on the electronic environment in the vicinity of the fluorine nuclei. ^{19}F resonances display a high degree of dispersion and are predictable with good precision from quantum calculations of electronic distributions (31). The proton distributions in the vicinity of the fluorine nuclei can also be established on the basis of hydrogen/deuterium primary isotope shifts of the ^{19}F resonances. For the F···H-N and F···H-O hydrogen bonds present between the MgF_3^- moiety and the protein (Fig. 2*B*), the magnitudes of the isotope shifts reflect the local proton densities because of the through-space transmission of the electric field differences between X-H and X-D bonds (32). Moreover, the proton distributions can be assessed independently through the quantitation of ^{19}F-^1H NOEs,

as were used in the solution structure determinations of the PGM-MgF_3-G6P-TSA and PGM-AlF_4-G6P-TSA complexes (8, 10). Together, these measurements provide a picture of the relationship between the charge distribution of the phosphoryl group transfer mimic and the protein.

To investigate the ability of ^{19}F NMR parameters to report on the environment within the active site of phosphoryl group transfer TSAs, three PGM-MgF_3-TSA complexes were prepared containing slightly differing sugar phosphates: G6P (PGM-MgF_3-G6P-TSA), 6-deoxy-6-(phosphonomethyl)-D-glucopyranoside (33) (PGM-MgF_3-phosphonate-TSA), and 2-deoxy-G6P (PGM-MgF_3-2deoxyG6P-TSA). Effective K_d values were determined through the titration of sugar phosphate solutions into separate solutions of β-PGM containing magnesium and fluoride and monitored using either ^1H NMR or isothermal titration calorimetry. Saturated complexes could be achieved for all three species (K_d: G6P = 1 μM, 2-deoxyG6P = 80 μM, 6-deoxy-6-(phosphonomethyl)-D-glucopyranoside = 300 μM). The ^{19}F NMR spectra of these PGM-MgF_3-sugar phosphate-TSA complexes prepared in 100% H_2O buffer and in 100% D_2O buffer are presented in Fig. 4. The three fluorine atoms in each of the MgF_3^- moieties are hydrogen bonded to multiple exchangeable donors of the protein, and a comparison of the spectra recorded in H_2O buffer and D_2O buffer allows the sum of the individual isotope shifts to be measured. In the PGM-MgF_3-G6P-TSA complex, F_A is coordinated by three protons, $L9H^N$, $D10H^N$, and $S114H^O$ (Fig. 2*B*), in a distorted tetrahedral arrangement, giving a sum isotope shift of 1.6 ppm. F_B and F_C have trigonal coordination involving two protons ($A115H^N$ and $K145H^{N\zeta}$) and one proton ($G6P\text{-}2'H^O$), respectively, and have correspondingly smaller sum isotope shifts (1.4 ppm and 0.9 ppm, respectively).

The PGM-MgF_3-G6P-TSA and the PGM-MgF_3-phosphonate-TSA complexes exhibit similar ^{19}F chemical shifts and isotope shifts indicating that replacement of the 6′-oxygen with a methylene group has only a minor effect on the relationship between the protein and the MgF_3^- moiety; the ^{19}F chemical shifts move

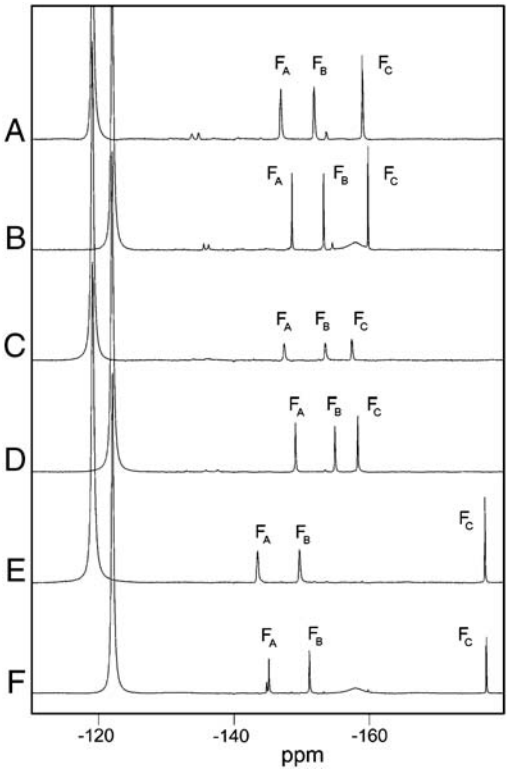

Fig. 4. ^{19}F NMR spectra of three PGM-MgF_3-sugar phosphate-TSA complexes. Spectra were recorded at 25 °C in 50 mM K^+ Hepes buffer at pH 7.2, in 100% H_2O or in 100% D_2O. Chemical shifts are given in ppm for each ^{19}F resonance in the complex. (*A*) PGM-MgF_3-G6P-TSA in 100% H_2O buffer ($F_A = -147.0$, $F_B = -151.8$, $F_C = -159.0$). (*B*) PGM-MgF_3-G6P-TSA in 100% D_2O buffer ($F_A = -148.6$, $F_B = -153.3$, $F_C = -159.8$). (*C*) PGM-MgF_3-phosphonate-TSA in 100% H_2O buffer ($F_A = -147.5$, $F_B = -153.5$, $F_C = -157.4$). (*D*) PGM-MgF_3-phosphonate-TSA in 100% D_2O buffer ($F_A = -149.1$, $F_B = -154.9$, $F_C = -158.3$). (*E*) PGM-MgF_3-2deoxyG6P-TSA in 100% H_2O buffer ($F_A = -143.5$, $F_B = -149.7$, $F_C = -177.1$). (*F*) PGM-MgF_3-2deoxyG6P-TSA in 100% D_2O buffer ($F_A = -145.2$, $F_B = -151.2$, $F_C = -177.3$) and with peak F_A showing evidence of residual proton occupancy at one β-PGM hydrogen bond donor site resulting from exchange protection in the D_2O buffer. Free F^- resonates at −119.0 ppm in 100% H_2O buffer and at −122.0 ppm in 100% D_2O buffer.

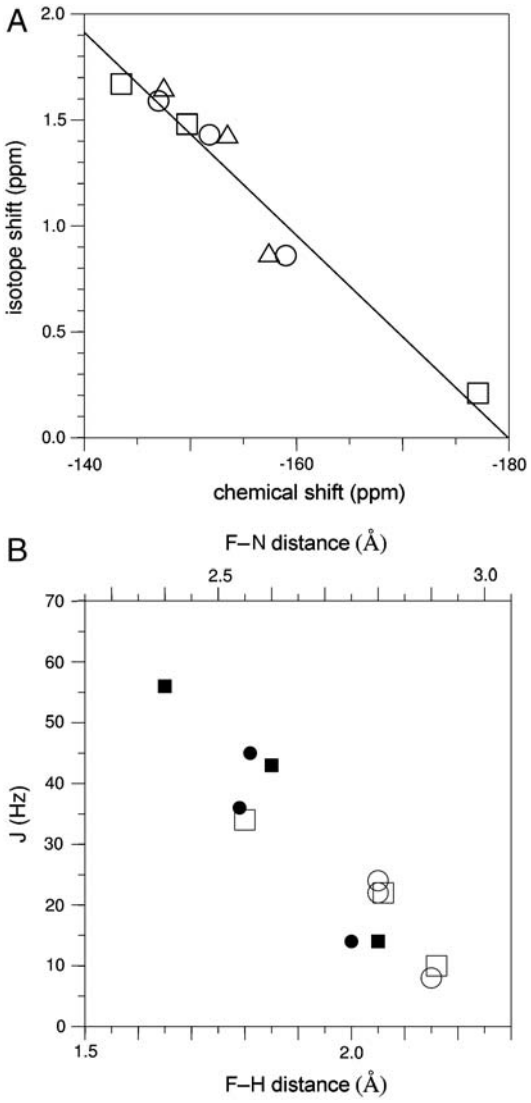

Fig. 5. Correlation of ^{19}F NMR parameters and their relationships to the crystalline state. (*A*) Correlation plot showing the relationship between chemical shift (ppm) and isotope shift ($\delta_{H_2O} - \delta_{D_2O}$, ppm) for the ^{19}F resonances of the PGM-MgF_3-G6P-TSA complex (*circles*), the PGM-MgF_3-phosphonate-TSA complex (*triangles*) and the PGM-MgF_3-2deoxyG6P-TSA complex (*squares*). Linear regression analysis gives $R^2 = 0.94$. (*B*) Correlation plot showing the relationships between J_{HF} (*filled symbols*) and J_{NF} (*open symbols*) couplings with the corresponding internuclear distances derived from structures of the PGM-MgF_3-G6P-TSA (*circles*) and PGM-AlF_4-G6P-TSA (*squares*) (10) complexes. The F-N distances are derived directly from the experimental coordinates, and the F-H distances are determined to hydrogens positioned using the program XPLOR.

slightly upfield for F_A (−0.5 ppm) and F_B (−1.7 ppm), but downfield for F_C (+1.6 ppm). The tetrahedrally coordinated fluorine, F_A, is barely affected, while for the trigonally coordinated fluorines, F_B and F_C, the small gain in electron density of the former is matched by a similar loss of electron density in the latter, indicative of a subtle shift in the position of the MgF_3^- moiety relative to the protein.

In contrast, the PGM-MgF_3-2deoxyG6P-TSA complex shows more dramatic changes in chemical shift compared with the PGM-MgF_3-G6P-TSA complex, with F_C moving substantially upfield (−18.1 ppm), while F_A and F_B move downfield, but to lesser extents (+3.5 ppm and +2.1 ppm, respectively). The magnitude of the chemical shift change, and the fall in isotope shift for F_C to close to zero (0.2 ppm), indicate that the removal of the sugar hydroxyl group, which otherwise would coordinate F_C, leaves this fluorine without hydrogen bonding (i.e. the trigonal coordination of F_C is not reestablished through hydrogen bonding to a water molecule). The consequence of the removal of a hydrogen-bonding partner for F_C is that F_A and F_B move slightly closer to their hydrogen-bonding partners, as evidenced by the small increase in sum isotope shifts for these fluorine atoms ($F_A = 1.7$ ppm and $F_B = 1.5$ ppm).

Collating all of the above data, it is also possible to establish that in general the measured ^{19}F chemical shifts correlate very well with the measured isotope shifts (Fig. 5*A*). This illustrates the dominant influence that the very local hydrogen-bonding groups have on shaping the charge density on the MgF_3^- moiety. To understand more fully the nature of the hydrogen bonding between the coordinating groups and the model of the transferring phosphate, it is also possible to measure scalar couplings associated with the F···H-N hydrogen bonds (Fig. S6). In the PGM-MgF_3-G6P-TSA complex, J_{HF} and J_{NF} couplings are observable for each amide group H^N···F pair, and the magnitudes of both couplings correlate closely with distances measured from crystal structure analysis (Fig. 5*B*). For example, the distortion of the tetrahedral coordination of F_A, in which protons $D10H^N$ and $S114H^O$ make an approximately trigonal arrangement while proton $L9H^N$ is positioned near the apex of a trigonal pyramid, is clearly reflected in the scalar coupling measurements. Hence, the scalar couplings provide further independent corroboration of the positions of nitrogens (and hydrogens) in the immediate vicinity of the transferring phosphate mimic.

The remarkable relationship between all of the observed NMR parameters and the coordinates determined in the crystalline state shows that, for the β-PGM complexes studied here, the atomic positions determined at high resolution in the solid phase reflect very closely the solution behavior. The NMR parameters also establish the nature of subtle changes in the structure when small changes in the constituency of the TSA complexes are made. In combination with our reevaluation of the crystalline state, these results leave no doubt that the transition-state-like complex for β-PGM has MgF_3^- coordinated between oxygen-1β of glucose 6-phosphate and a γ-oxygen of D8 in the protein active site in solution and in the solid phase. There is no evidence that supports the presence of a pentacoordinate phosphorane (17) under any conditions. Unrestrained reanalysis of the electron density generates a TBP with corrected bond lengths appropriate for Mg-F and not P-O bonds, and the anomalous dispersion data show that the central atom is not phosphorus. Furthermore, β-PGM can neither maintain a stable long-lived aspartyl phosphate, nor be phosphorylated by Pi, as had been postulated previously (14). However, the metal fluoride complexes offer opportunities to measure properties of near-TS complexes that are currently unmeasureable for phosphorus oxide species, in particular the independent measures of local electrostatic and hydrogen-bonding distributions using ^{19}F NMR.

Materials and Methods

Details of all of the procedures are provided in the *SI Text*.

Crystallographic Methods. Native β-PGM was crystallized by vapor diffusion from a buffer containing 50 mM K^+ Hepes pH 7.2, 5 mM $MgCl_2$, 1 mM NaN_3 and 0.1 mM DTT with 26–30% PEG 4000, 200 mM sodium acetate, and 100 mM Tris pH 7.5 as precipitants. For the PGM-MgF_3-G6P-TSA complex, 10 mM NH_4F and 5 mM G6P were added and the precipitants were 19–21% PEG 3350 and 50 mM magnesium acetate. Diffraction data were collected from cryocooled crystals to 1.55 Å (native) and 1.3 Å (TSA) resolution at the European Synchrotron Radiation Facility (ESRF) and the structures were solved by molecular replacement. Ligands in the PGM-MgF_3-G6P-TSA complex were not included in the refinement until the final rounds so they could be built into unbiased difference Fourier maps. For the final round of refinement, restraints for the MgF_3^- moiety were relaxed allowing the exact atomic positions to be defined. A long-wavelength dataset was collected to 2.0 Å on a crystal of the PGM-MgF_3-G6P-TSA complex at a wavelength of 1.77 Å ($E = 7$ keV) to exploit the anomalous signal from phosphorus.

NMR Methods. ^{31}P spectra were acquired at 291 K on a sample of β-PGM containing 0.5 mM β-PGM, 10 mM $MgCl_2$, 5 mM G6P, 1 mM DTT, in 1 mM K^+ Hepes buffer at pH 7.5. ^{31}P spectra were acquired on the PGM-MgF_3-G6P-TSA complex at 298 K, the sample containing 2 mM β-PGM, 5 mM $MgCl_2$, 10 mM NH_4F, 5 mM G6P, 2 mM NaN_3, in 50 mM K^+ Hepes buffer at pH 7.2. ^{19}F NMR experiments were recorded at 298 K on samples prepared separately in both 50 mM K^+ Hepes buffer in 100% H_2O pH 7.2 and 50 mM K^+ Hepes buffer in 100% D_2O pH 7.2 (uncorrected for D_2O effects), and contained 0.5 mM β-PGM, 5 mM $MgCl_2$, 10 mM NH_4F, 2 mM NaN_3, and either 5 mM G6P (PGM-MgF_3-G6P-TSA), 5 mM 2-deoxy-G6P (PGM-MgF_3-2deoxyG6P-TSA) or 5 mM 6-deoxy-6-(phosphonomethyl)-D-glucopyranoside (PGM-MgF_3-phosphonate-TSA). 6-deoxy-6-(phosphonomethyl)-D-glucopyranoside was synthesized as described previously (33). In the 100% H_2O buffer experiments, the lock was provided by D_2O sealed inside a capillary inserted in the NMR sample tube. ^1H, ^{15}N heteronuclear single quantum coherence (HSQC) experiments were recorded under the same conditions, except that 10% D_2O was added as an internal lock.

ACKNOWLEDGMENTS. We thank Steve Gamblin for helpful discussions and preliminary crystallization work. This research was supported by the Biotechnology and Biological Sciences Research Council and the Mizutani Foundation for Glycoscience.

1. Schroeder GK, Lad C, Wyman P, Williams NH, Wolfenden R (2006) The time required for water attack at the phosphorus atom of simple phosphodiesters and of DNA. *Proc Natl Acad Sci USA* 103:4052–4055.
2. Lad C, Williams NH, Wolfenden R (2003) The rate of hydrolysis of phosphomonoester dianions and the exceptional catalytic proficiencies of protein and inositol phosphates. *Proc Natl Acad Sci USA* 100:5607–5610.
3. Friedhoff P, et al. (1996) Kinetic analysis of the cleavage of natural and synthetic substrates by the *Serratia* nuclease. *Eur J Biochem* 241:572–580.
4. Stec B, Hehir MJ, Brennan C, Nolte M, Kantrowitz ER (1998) Kinetic and x-ray structural studies of three mutant *E. coli* alkaline phosphatases: Insights into the catalytic mechanism without the nucleophile Ser102. *J Mol Biol* 277:647–662.
5. Harder KW, et al. (1994) Characterization and kinetic analysis of the intracellular domain of human protein tyrosine phosphatase beta (HPTP beta) using synthetic phosphopeptides. *Biochem J* 298:395–401.
6. Cleland WW, Hengge AC (2006) Enzymatic mechanisms of phosphate and sulfate transfer. *Chem Rev* 106:3252–3278.
7. Graham DL, et al. (2002) MgF_3^- as a transition state analog of phosphoryl transfer. *Chem Biol* 9:375–381.
8. Baxter NJ, et al. (2006) A Trojan horse transition state analogue generated by MgF_3^- formation in an enzyme active site. *Proc Natl Acad Sci USA* 103:14732–14737.
9. Lee JY, Yang W (2006) UvrD helicase unwinds DNA one base pair at a time by a two-part power stroke. *Cell* 127:1349–1360.
10. Baxter NJ, et al. (2008) Anionic charge is prioritized over geometry in aluminum and magnesium transition state analogs of phosphoryl transfer enzymes. *J Am Chem Soc* 130:3952–3958.
11. Frey PA, Hegeman AD (2007) *Enzymatic Reaction Mechanisms* (Oxford Univ Press, New York), pp 341–343.
12. Ray WJ, Jr, Long JW, Owens JD (1976) An analysis of the substrate-induced rate effect in the phosphoglucomutase system. *Biochemistry* 15:4006–4017.
13. Lahiri SD, Zhang G, Dunaway-Mariano D, Allen KN (2002) Caught in the act: The structure of phosphorylated β-phosphoglucomutase from *Lactococcus lactis*. *Biochemistry* 41:8351–8359.
14. Zhang G, et al. (2005) Catalytic cycling in β-phosphoglucomutase: A kinetic and structural analysis. *Biochemistry* 44:9404–9416.
15. Goličnik M, et al. (2009) Kinetic analysis of β-phosphoglucomutase and its inhibition by magnesium fluoride. *J Am Chem Soc* 131:1575–1588.

16. Lewis RJ, Brannigan JA, Muchova K, Barak I, Wilkinson AJ (1999) Phosphorylated aspartate in the structure of a response regulator protein. *J Mol Biol* 294:9–15.
17. Lahiri SD, Zhang G, Dunaway-Mariano D, Allen KN (2003) The pentacovalent phosphorus intermediate of a phosphoryl transfer reaction. *Science* 299:2067–2071.
18. Blackburn GM, Williams NH, Gamblin SJ, Smerdon SJ (2003) Comment on "The pentacovalent phosphorus intermediate of a phosphoryl transfer reaction". *Science* 301:1184c.
19. Webster CE (2004) High-energy intermediate or stable transition state analogue: Theoretical perspective of the active site and mechanism of β-phosphoglucomutase. *J Am Chem Soc* 126:6840–6841.
20. Allen KN, Dunaway-Mariano D (2003) Response to comment on "The pentacovalent phosphorus intermediate of a phosphoryl transfer reaction". *Science* 301:1184d.
21. Tremblay LW, Zhang G, Dai J, Dunaway-Mariano D, Allen KN (2005) Chemical confirmation of a pentavalent phosphorane in complex with β-phosphoglucomutase. *J Am Chem Soc* 127:5298–5299.
22. Lu Z, Dunaway-Mariano D, Allen KN (2008) The catalytic scaffold of the haloalkanoic acid dehalogenase enzyme superfamily acts as a mold for the trigonal bipyramidal transition state. *Proc Natl Acad Sci USA* 105:5687–5692.
23. Dai J, et al. (2009) Analysis of the structural determinants underlying discrimination between substrate and solvent in β-phosphoglucomutase catalysis. *Biochemistry* 48:1984–1995.
24. Lahiri SD, Zhang G, Radstrom P, Dunaway-Mariano D, Allen KN (2002) Crystallization and preliminary x-ray diffraction studies of β-phosphoglucomutase from *Lactococcus lactis*. *Acta Crystallogr* D58:324–326.
25. James TL (1985) Phosphorus-31 NMR as a probe for phosphoprotein. *Crit Revs Biochem* 18:1–30.
26. Quin LD *A Guide to Organophosphorus Chemistry* (John Wiley and Sons, Inc., New York), pp 169–203 p 341.
27. Sternweis PC, Gilman AG (1982) Aluminum: A requirement for activation of the regulatory component of adenylate cylase by fluoride. *Proc Natl Acad Sci USA* 79:4888–4891.
28. Wittinghofer A (1997) Signaling mechanistics: Aluminum fluoride for molecule of the year. *Curr Biol* 7:R682–R685.
29. Hao H, et al. (2002) Access to the structures of fluoromagnesium compounds: synthesis and structural characterization of the β-diketiminatomagnesium fluoride $[\{CH(CMeNAr)_2\}Mg(\mu\text{-}F)(THF)]_2$ toluene. *J Fluorine Chem* 115:143–147.
30. Schramm VL (2005) Enzymatic transition states and transition state analogues. *Curr Opin Struct Biol* 15:604–613.
31. Oldfield E (2005) Quantum chemical studies of protein structure. *Phil T Roy Soc B* 360:1347–1361.
32. Sonicki JG, Langaard M, Hansen PE (2007) Long-range deuterium isotope effects on C chemical shifts of intramolecularly hydrogen-bonded N-substituted 3-(cycloamine) thiopropionamides or amides: A case of electric field effects. *J Org Chem* 72:4108–4116.
33. Berkowitz DB, Bose M, Pfannenstiel TJ, Doukov T (2000) α-Fluorinated phosphonates as substrate mimics for glucose 6-phosphate dehydrogenase: The CHF stereochemistry matters. *J Org Chem* 65:4498–4508.